



Laser-Induced Forward Transfer of Silver Nanoparticles for a Black Metal Absorber

Ruo-Zhou Li^{1,2}, Lvjiu Guo¹, Leilei Liu^{2,3}, Mingqing Yang¹, Yuming Fang¹, Ying Yu^{1,2*} and Jing Yan^{3*}

¹College of Integrated Circuit Science and Engineering, Nanjing University of Posts and Telecommunications, Nanjing, China, ²National and Local Joint Engineering Laboratory of RF Integration and Micro Assembly Technology, Nanjing University of Posts and Telecommunications, Nanjing, China, ³College of Electronic and Optical Engineering, Nanjing University of Posts and Telecommunications, Nanjing, China

OPEN ACCESS

Edited by:

Andong Wang,
CNRS, France

Reviewed by:

Lu Hongbo,
Hefei University of Technology, China
Yifan Liu,
Microsoft, United States

*Correspondence:

Ying Yu
ying_yu_001@163.com
Jing Yan
jing.yan@njupt.edu.cn

Specialty section:

This article was submitted to
Optics and Photonics,
a section of the journal
Frontiers in Physics

Received: 29 April 2022

Accepted: 16 May 2022

Published: 24 June 2022

Citation:

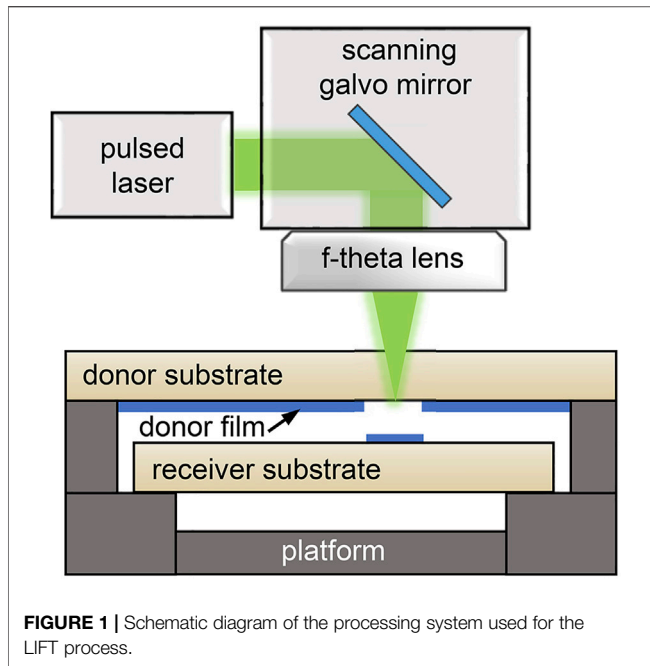
Li R-Z, Guo L, Liu L, Yang M, Fang Y,
Yu Y and Yan J (2022) Laser-Induced
Forward Transfer of Silver
Nanoparticles for a Black
Metal Absorber.
Front. Phys. 10:932050.
doi: 10.3389/fphy.2022.932050

Plasmonic nanostructures emerged as an appealing approach for black metal absorbers (BMAs) to provide significant light absorption. We present the simple and rapid fabrication of BMAs using laser-induced forward transfer of silver nanoparticles (AgNPs). Randomly distributed plasmon silver nanostructures at a multiscale were produced simultaneously during laser transfer, providing significant light absorption and antireflection features. The laser-transferred BMAs exhibit excellent absorption capacity of a value over 96% and a minimum reflection of 0.38%. A high scanning speed of 10 m/s was used that can complete the laser-induced forward transfer (LIFT) process within 2 s for a 1 cm² area. The nearfield light confinement is discussed in terms of the morphology of the obtained nanostructures. Photothermal conversion with macroscale temperature rising was demonstrated for the LIFT process is an effective method for the industrial production of BMAs with excellent absorption capacity.

Keywords: laser-induced forward transfer, silver nanoparticles, black metal absorber, plasmonic nanostructure, light absorption

INTRODUCTION

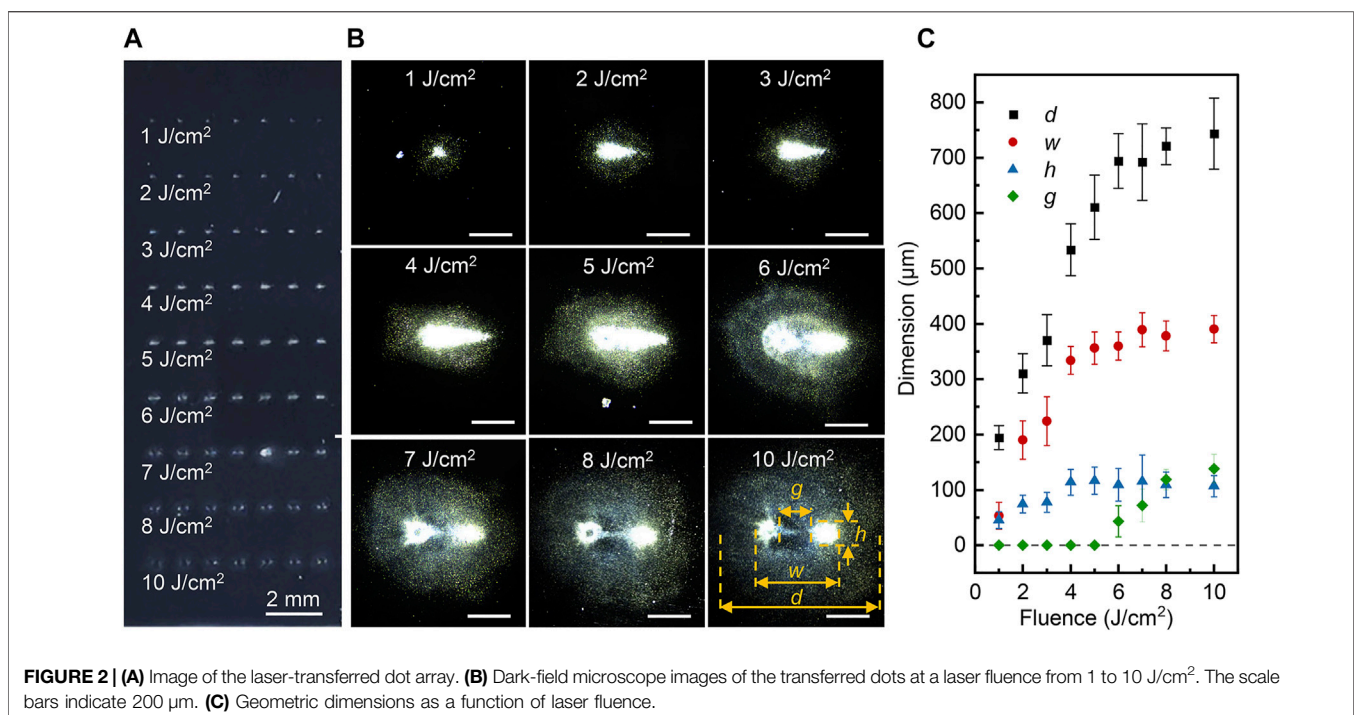
Plasmonic nanostructures emerged as an appealing approach for the black metal absorber (BMA) to provide significant light trapping and photothermal conversion in broadbands from near-ultraviolet to infrared for tremendous demands in applications such as water desalination [1, 2], antireflection [3–5], solar energy harvest [6–8], and thermal actuators [9]. The nanostructured metals enable complicated subwavelength electromagnetic interactions with light that significantly enhance the absorption of photon energy, yielding ‘black’ appearances on the macroscale [8]. Within this process, the localized surface plasmon resonance (LSPR) mechanism is typically employed to collect light from an absorption cross section prominently larger than the physical dimensions and to confine light energy into nanoscale ‘hotspots’ in-between adjacent nanostructures [10, 11]. The following non-radiative damping process of the generated hot electrons leads to strong light absorption and a possible generation of electron or heat energy [12, 13]. The involved physical effects highly depend on the morphologic, dimensional, and material characteristics of the plasmonic structures in BMAs. Therefore, considerable efforts aim to construct BMAs and engineer their morphologies for enhanced light-management capability from macro to nanoscale in broad wavelength coverage [5–8, 10].

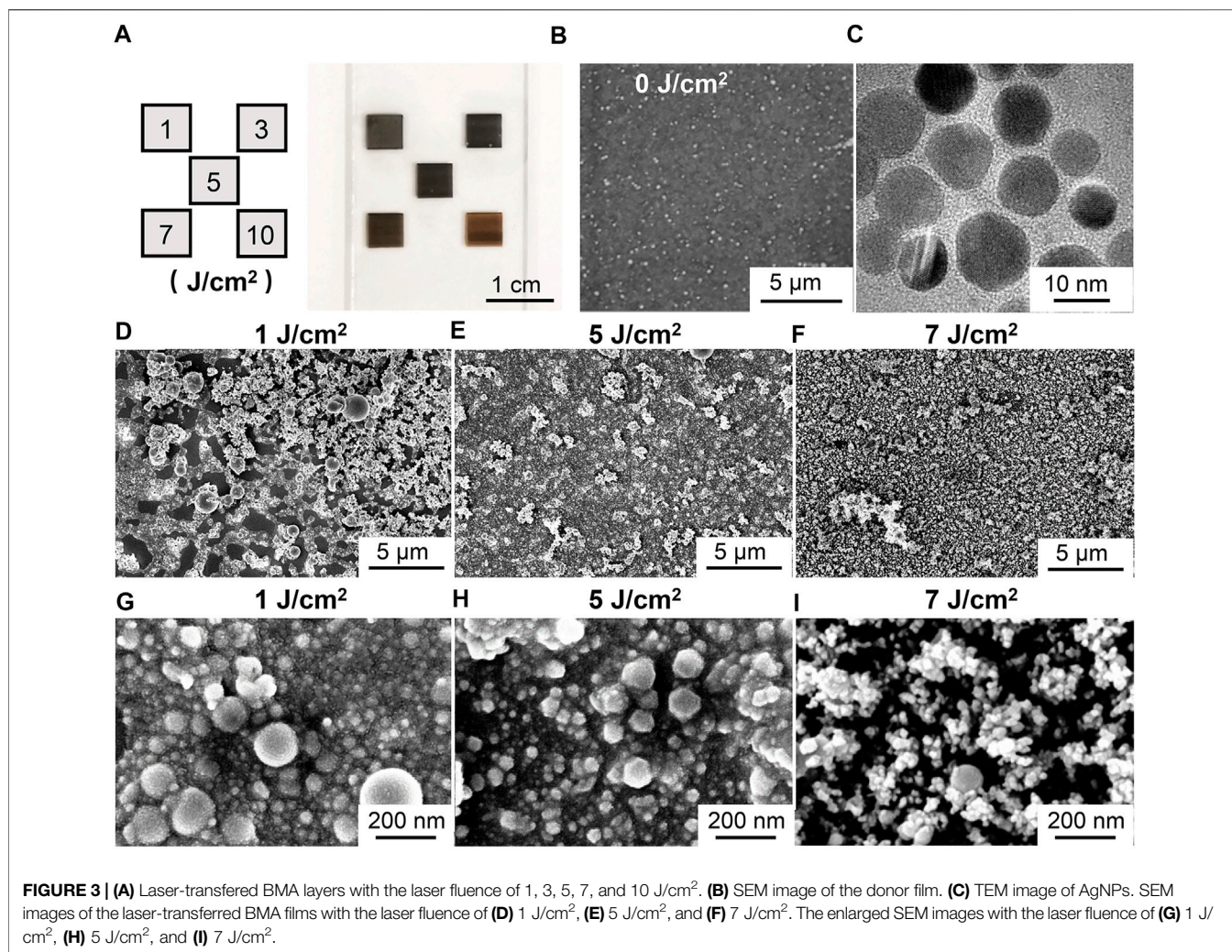


The fabrication of BMAs moves toward enhanced performance, lower material consumption, declined cost, and higher productivity ways. Lithographic technologies typically yield well-ordered elemental plasmonic nanostructures [10]. Meantime, processes such as chemosynthesis [4], self-assembly [1], transfer printing [14], and laser direct writing (LDW) [5, 6, 15–17] were used as alternatives with the possibility of yielding orderly or randomly distributed metal nanostructures with

fascinating broader absorption bands. Among these processes, LDW can fabricate micro–nano metal structures *in situ* on the target surfaces in a high-resolution, large-scale, cost-effective, and rapid manner that fulfills the industrial prospects [16, 18–21]. Highly reflective metal surfaces can be tuned to black metals by laser inducing well-controlled metallic structures at a multiscale [5]. In some dual-scale structures, the larger features function as the skeleton of the entire surface architecture, while the finer sub-structures fill or cover the skeleton. The synergetic effects of micro–nano hierarchical metal structures [6] provide suppressive external reflection, enhanced light trapping, and abundant nanoscale hotspots for absorption [22]. Despite these advantages, laser fabrication of BMAs involves protocols such as laser ablation and laser-induced dewetting [15, 16], whereas laser-induced forward transfer (LIFT) of metal nanostructures for BMAs has not been reported yet.

Apart from laser ablation and laser-induced dewetting methods that directly modify the surface morphology of the sample surface, LIFT is an additive process that employs laser pulses to push a fraction of materials from a donor film toward an acceptor substrate [18, 23–25]. Metallic materials including high-viscosity silver pastes [25] and silver nanoinks [26, 27] demonstrate a variety of applications such as diffractive microstructures, conductive interconnections, and flexible electronics. Here, in this article, we present the simple and rapid fabrication of BMAs using laser-induced forward transfer of silver nanoparticles (AgNPs). Randomly distributed plasmon silver nanostructures at multiscale were produced simultaneously during laser transfer, providing significant light absorption and anti-reflection features. A high scanning speed of 10 m/s was used that can complete the LIFT process within 2 s for a 1 cm² area. The nearfield light confinement is discussed in terms





of the morphology of the obtained nanostructures. Photothermal conversion with macroscale temperature rising was demonstrated for the laser-induced BMAs.

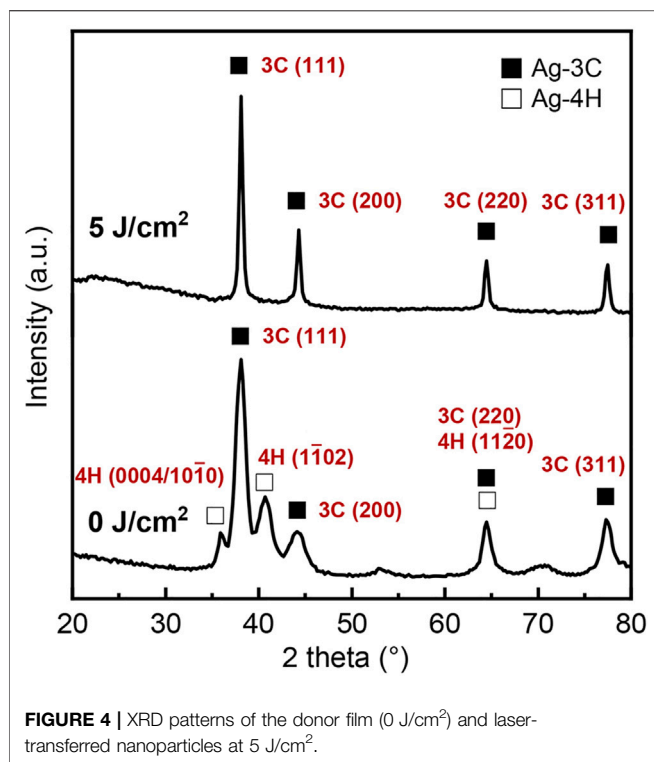
EXPERIMENTAL

Figure 1 shows the schematic diagram of the processing system used for the LIFT process. A commercial nanosecond (ns) laser with a wavelength of 1,024 nm and a pulse duration of 20 ns was used to fabricate the BMA at a fixed repetition rate of 110 kHz. The laser beam was deflected by a high-speed scanning galvo mirror and was focused by an f-theta lens with a focal length of 100 mm. The laser beam passed through the transparent donor glass substrate onto the surface of a donor film. The donor film used was prepared from a commercially available silver nanoink (UTAg40 TE, UT Dots Inc.). The solid content of the ink was 40% w/v with nanoparticles of an average particle size of 10 nm. For each donor substrate, the ink with a volume of 20 μ L was spin-coated onto a microscope glass slide at 500 rpm for 30 s and then dried on a hotplate at 50°C for 5 min. Microscope glass slides were

used as the receiver substrates. The gap between the donor and receiver substrates was adjusted to 50 μ m.

The LIFT was performed at an ambient air environment and room temperature with a high-scanning speed of 10 m/s. To fabricate BMAs (areal transfer), a laser bidirectional scanning strategy was used with a hatch distance of 10 μ m. Therefore, the LIFT process can be accomplished within 2 s for a full scan of 1 cm² area. The laser fluence is defined as the total laser energy per area; hereby, the laser fluence of the areal transfer was in the range between 1 J/cm² and 10 J/cm². For the dot transfer, multiple pulse irradiations were used with the pulse energy varying from 9.1 to 90.9 μ J in corresponding to laser fluence from 1 to 10 J/cm² in the areal transfer.

The morphologies of the nanoparticles and microstructures were characterized using a transmission electron microscope (ZEISS LIBRA200) and a scanning electron microscope (ZEISS Gemini500). Microscopic observations were conducted using an optical microscope (Olympus BX53M). The X-ray diffraction (XRD) patterns were obtained *via* an X-ray diffractometer (PANalytical Empyrean XRD) with a Cu K α radiation source ($\lambda = 1.5406$ Å). The optical spectra were measured using a fiber



optic spectrometer (B&W Tek Quest X) equipped with an integrating sphere (Thorlabs 2P4) to observe the scattered light. **Supplementary Figure S1** sketches the optical setup of the transmission and reflection measurements. The absorption (A) is obtained by deducing the measured transmission (T) and reflection (R) according to the formula $A=1-R-T$. The thermal observations were performed by using a thermal imaging camera (FOTRIC 222s).

RESULTS AND DISCUSSION

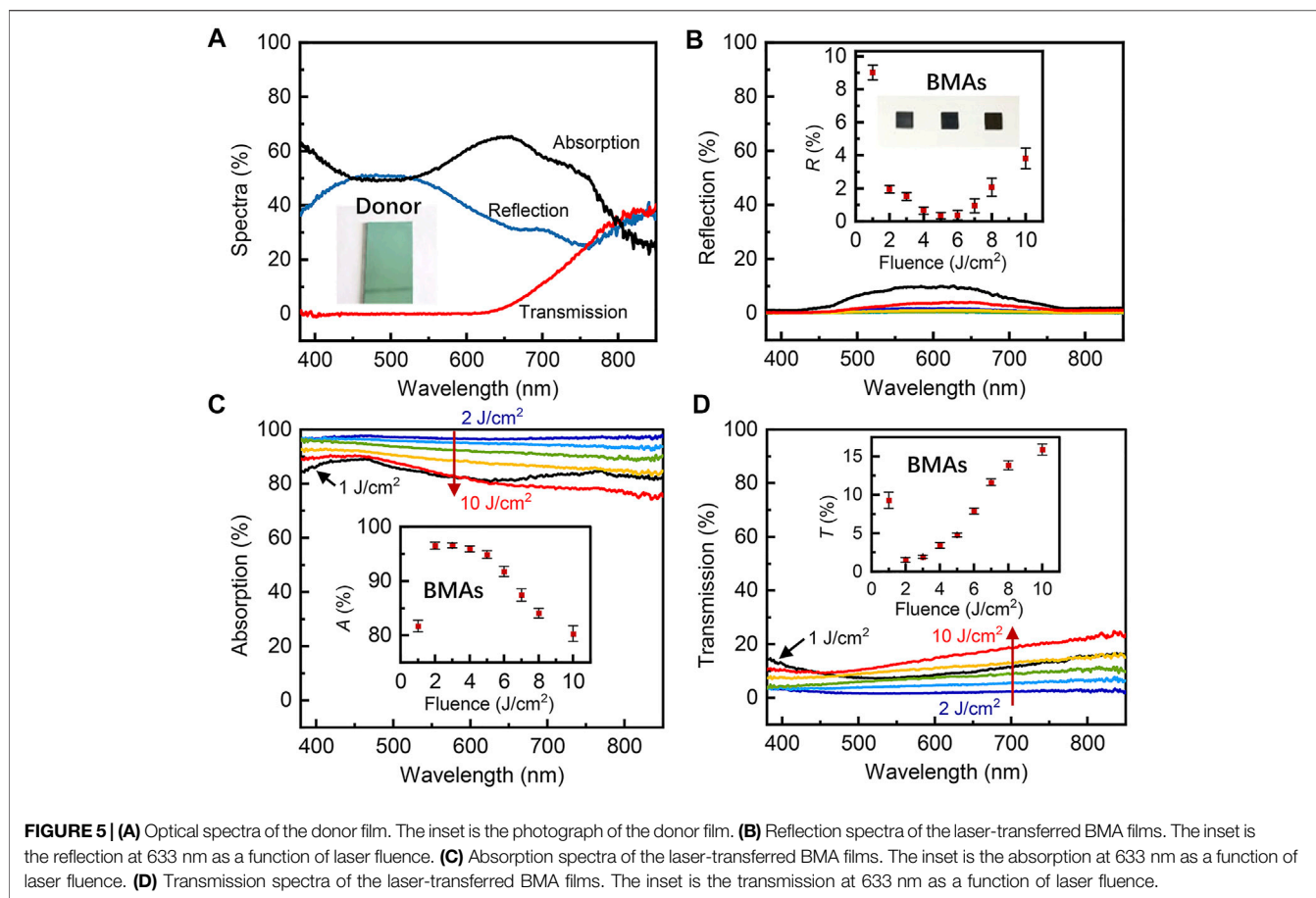
Laser-Transferred Silver Nanostructures

The first experiments were conducted to study the effect of laser fluence. Dot deposition was performed under dynamic conditions with a constant scanning speed of 10 m/s (consistent with the scene of BMA fabrication). A 7×9 single dot array was successfully transferred with various pulse energy sets (**Figure 2A**). The dark-field microscope images in **Figure 2B** show the detailed morphologies of the transferred dots. The printed dots were converted from a roughly circular shape to a comet shape as the laser fluence increased from 1 to 5 J/cm^2 . Further increase in laser fluence leads to gaps in the middle of the printed dots, even slicing the comet-shaped dots into two divided regions. Meanwhile, some splashes and debris appear around the dots. The phenomenon of splashing and debris is more pronounced in a higher laser fluence. **Figure 2C** quantitatively plots the geometric dimensions (the length w and width h of the printed dots, the diameter d of the splashed area, and the width g of the gap, as indicated in **Figure 2B**) as a function of pulse

energies. The deviations of the dots at the same set of laser parameters are due to the slight variations in the laser power and donor film thickness. The dimensions show approximately linear growth trends at a laser fluence below 5 J/cm^2 without ablated gaps. At a laser fluence above 6 J/cm^2 , the ablated gaps formed and broadened rapidly with average widths up to $138 \mu\text{m}$. Meanwhile, the increase in the other dimensions slows down. Control over the dot profiles and dimensions was achieved.

The obtained comet-shaped dots at the receiver substrate are consistent with the distribution of the multiple pulses irradiated at the donor film that were confirmed by the microscopic images (**Supplementary Figure S2**). The high scanning speed of the galvo mirror leads to an inline distribution of the laser pulses. Meanwhile, the high laser fluence and the asymmetrical laser pulse duration (with a typical steep rising edge of 15 ns and a moderate falling edge of 75 ns) may lead to anisotropic ejection [28] of the transferred material and complex propagation of shockwaves [29] as the laser pulse impacts the donor film. The shockwave has significant effects on the transferred material, which is evidenced by the incremental surrounding splashing and debris at increased laser fluence. Therefore, the formation of the comet-shaped dots may be due to the synergic effects of the aforementioned factors. The gaps, which appeared at a laser fluence above 6 J/cm^2 , are typically attributed to laser ablation [30] since the intensive shockwaves are possible to damage and remove the transferred materials in the vicinity of the focal point. Also, laser pulses punch holes in the donor film, and the successive laser pulses can directly irradiate the obtained receiver substrate that can ablate the obtained Ag nanostructures. This may also lead to an enlarged splash area. The investigations of the aforementioned dynamics, however, fell beyond the scope of the present study.

AgNPs were deposited into a uniform silver nanostructure layer by areal transfer, as shown in **Figure 3A**. The surface reflection of glass slides was suppressed with black appearances. The morphology of the donor film and obtained silver nanostructures on the receiver substrates with some typical laser fluence are shown in SEM images in **Figures 3B–I**. The images reveal that the LIFT process directly influences the geometry of the AgNPs from continuous AgNP films to fragmented silver nanostructures. For the low laser fluence such as 1 J/cm^2 (**Figures 3D,G**) and 5 J/cm^2 (**Figures 3E,H**), the BMA layers contain considerable AgNPs with wide size distributions from 10 nm to $2 \mu\text{m}$. Some aggregates, which refer to the assemblages of AgNPs, were several micrometers in size and randomly distributed on the receiver glass slide surface. Considering the particle size of the donor film to be 10 nm and homogeneous, the larger AgNPs were formed through photothermal sintering and melting mechanism during the laser irradiation [31]. It should be noted that the 5 J/cm^2 case shows a more continuous BMA layer than the porous film in the 1 J/cm^2 case. Higher laser fluence levels result in uniform distributed AgNP aggregates with reduced sizes to the sub-micrometer scale. Meanwhile, the large AgNPs with sizes from several hundred micrometers to several micrometers can be rarely seen. This may be attributed to the smashing of the Ag fragments into smaller pieces, and the enhanced laser ablation



effects which are revealed in the dot transfer observations. Further increase in the laser fluence leads to a non-uniform silver layer as illustrated in **Supplementary Figure S3**. Generally, these micro/nano-sized particles and fractional aggregates form multiscale three-dimensional (3D) nanostructures for BMAs, and the morphology can be tuned by laser fluence from the porous layer containing multiscale AgNPs and large aggregates (1 J/cm^2), to similar but continuous membrane (5 J/cm^2) and to uniform distributed aggregates (7 J/cm^2).

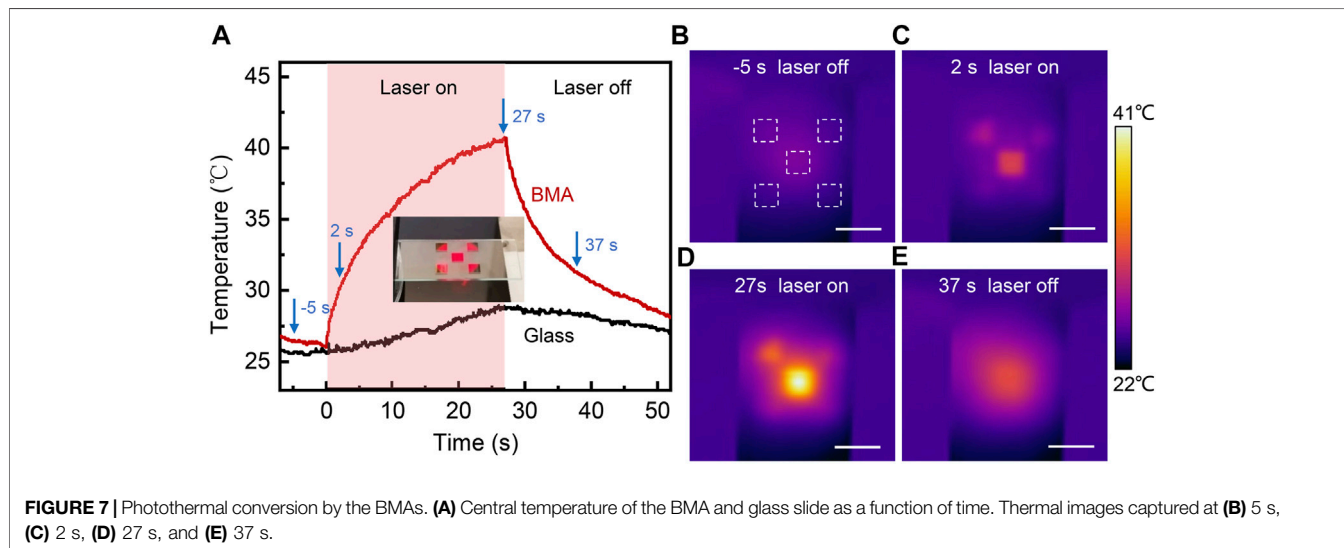
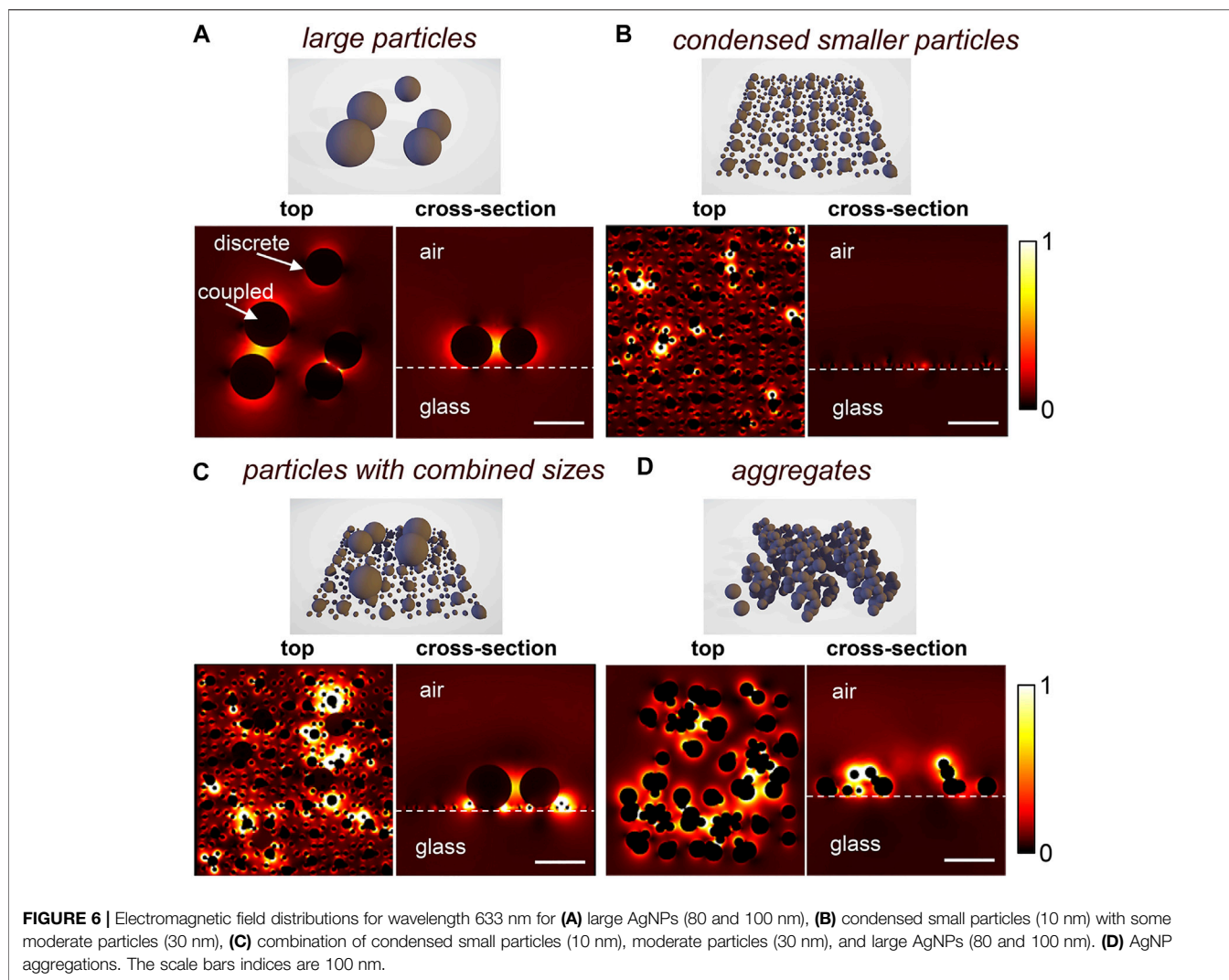
XRD patterns in **Figure 4** compare the crystalline phases of the donor film and the laser-transferred BMA layer. The donor film consists of 10 nm AgNPs and has the peaks corresponding to (111), (200), (220), and (311) planes spacing of the cubic (3C) phase with three additional peaks corresponding to the metastable hexagonal (4H) phase of silver. It should be noted that an obvious 4H to 3C phase transition can be confirmed in the pattern at 5 J/cm^2 and other laser fluences (**Supplementary Figure S4A**), revealing that an increase in temperature may occur during the laser irradiation because the stability of 4H decreases at higher temperatures [32]. A significant rise in the intensity ratio between (200) and (111) peaks can be found in **Supplementary Figure S4B**, in accordance with the sintering and melting of the AgNPs during the LIFT process with the formation of larger nanostructures [33]. Only slight variations of the ratio are observed at various laser fluences. It has been

previously verified that the finally obtained BMAs have a typical 3C silver nanocrystal feature, whereby photothermal-induced sintering and melting play a role in the laser transfer process.

Light Absorption of BMAs

The light absorption properties of the AgNP donor film and the laser-transferred BMAs on glass slides are illustrated in **Figure 5**. Intrinsically, the AgNP donor film surfaces exhibit a shining greenish appearance as the inset shown in **Figure 5A**. Its reflection spectrum exhibits a maximum value of 51% at around 480 nm with limited absorption. In contrast, laser-transferred BMAs dramatically suppress the reflection (**Figure 5B**) due to the significantly enhanced absorption (**Figure 5C**). At a laser fluence of 3 J/cm^2 , the absorption has a maximum value of over 96% level throughout all wavelengths from 380 to 850 nm. The corresponding reflection is below 1.69%. As the laser fluence increase, the BMAs shows some slight decrease in the reflection with a minimum value of sub 0.38% level at a laser fluence of 5 J/cm^2 . Further increase in the laser fluence leads to enhanced reflection, reduced absorption, and ultimately enlarged transmission (**Figure 5D**).

Generally, the multiscale metal structures can enhance the light trapping effect and render the surfaces strong antireflection



characteristics [17]. The light trapping and LSPR are highly dependent on their particular morphologic features. Simulation results obtained by the 3D finite element method (FEM) are compared in **Figure 6**, with four typical morphologies in accordance with the samples in the present study, that is, discrete large AgNPs of 80–100 nm in size (**Figure 6A**) and condensed small particles of 10 nm in size with some moderate particles of 30 nm in size (**Figure 6B**) that is similar to the donor film case (**Figure 3B**), a combination of aforementioned large AgNPs and condensed smaller particles (**Figure 6C**), which is similar to the 1 and 5 J/cm² cases (**Figures 3G,H**), and aggregations (**Figure 6D**) that exist in the 1–7 J/cm² cases (**Figures 3D–F**). The nanoparticles were colored as black spheres to improve visibility in the electric distribution figures. It can be seen that the particles with combined sizes and the aggregates can provide more condensed hotspots than the case with large particles and the case that contains only smaller particles.

It is known that AgNPs can form the LSPR phenomenon (**Figure 6A**), where the absorption bands are usually narrow. The coupling between adjacent particles further enhances the absorption bands and provides an improved field enhancement with bright hotspots in the narrow gaps [4]. The donor film (**Figure 3B**) of condensed small particles (10 nm) with some larger particles (30 nm) on the top shows randomly distributed tiny hot spots (**Figure 6B**), providing the absorption over a wide wavelength range. However, the simplex structure can only result in limited properties, which is consistent with the spectra of the donor film in **Figure 5A**. Therefore, for the laser-transferred BMAs with randomly distributed structures (**Figures 3D–I**), two more factors are further attributed to the excellent absorption characteristics. First, the synergetic effects of multiscale AgNPs generally possess abundant 3D hotspots in multi-sizes (**Figure 6C**) and spaces. Second, the Ag aggregates provide larger and more complex 3D morphologies that enable stronger coupling among aggregates and AgNPs (**Figure 6D**). Ultimately the synergetic effects of the multiscale particles and aggregates enhance the absorption that makes laser-transferred silver black.

A demonstration was provided to show the photothermal conversion by laser-transferred BMAs. Under laser (633 nm, 400 mW/cm²) illumination of the sample shown in **Figure 2A** and the inset in **Figure 7A**, the temperature at the BMA surface increased rapidly to a value of 40.8°C in 27 s. **Figures 7B–E** verified the light-to-heat conversing enhancement of the BMAs with a distinct temperature boundary between the BMA area and the bare glass slide area. Heat dispersion was also observed as the decrease in the surface temperature when the laser was off. The heat dispersions also blur the sharpness of the thermal pattern. The images taken by the thermal imaging camera also exhibit the uniformity of the transferred BMAs.

CONCLUSION

Herein, we present the simple and rapid fabrication of BMAs using laser-induced forward transfer of silver nanoparticles (AgNPs). Randomly distributed plasmon silver nanostructures at a multiscale were produced simultaneously during laser transfer, providing significant light absorption and antireflection features. The laser-transferred BMAs exhibit excellent absorption capacity of a value over 96% and a minimum reflection of 0.38%. A high scanning speed of 10 m/s was used that can complete the LIFT process within 2 s for a 1 cm² area. The nearfield light confinement is discussed in terms of the morphology of the obtained nanostructures, revealing that the LSPR phenomenon, the synergetic effects of multiscale AgNPs, and the complex 3D morphologies of the aggregations can be attributed to the high absorption. Photothermal conversion with macroscale temperature rising was demonstrated for the laser-induced BMAs. The results indicated that LIFT is an effective method for the industrial production of BMAs with excellent absorption capacity.

DATA AVAILABILITY STATEMENT

The raw data supporting the conclusion of this article will be made available by the authors, without undue reservation.

AUTHOR CONTRIBUTIONS

R-ZL and JY directed and wrote the manuscript, and R-ZL, LG, and MY conducted the experiments. YY directed and supervised the research. LL and YF contributed toward significant discussions and revised the manuscript. All authors contributed to the manuscript and approved the submitted version.

FUNDING

This work was supported by the National Natural Science Foundation of China under the grant nos. 61704090 and 11904177, and the National and Local Joint Engineering Laboratory of RF Integration and Micro-Assembly Technology under the grant no. KFJJ20210205.

SUPPLEMENTARY MATERIAL

The Supplementary Material for this article can be found online at: <https://www.frontiersin.org/articles/10.3389/fphy.2022.932050/full#supplementary-material>

REFERENCES

- Zhou L, Tan Y, Wang J, Xu W, Yuan Y, Cai W, et al. 3d Self-Assembly of Aluminium Nanoparticles for Plasmon-Enhanced Solar Desalination. *Nat Photon* (2016) 10(6):393–8. doi:10.1038/nphoton.2016.75
- Kiriarachchi HD, Awad FS, Hassan AA, Bobb JA, Lin A, El-Shall MS. Plasmonic Chemically Modified Cotton Nanocomposite Fibers for Efficient Solar Water Desalination and Wastewater Treatment. *Nanoscale* (2018) 10(39):18531–9. doi:10.1039/c8nr05916k
- Zheng B, Wang W, Jiang G, Mei X. Fabrication of Broadband Antireflective Black Metal Surfaces with Ultra-light-trapping Structures by Picosecond Laser Texturing and Chemical Fluorination. *Appl Phys B* (2016) 122(6):180. doi:10.1007/s00340-016-6449-1
- Zhang X-Y, Shan F, Zhou H-L, Su D, Xue X-M, Wu J-Y, et al. Silver Nanoplate Aggregation Based Multifunctional Black Metal Absorbers for Localization, Photothermal Harnessing Enhancement and Omnidirectional Light Antireflection. *J Mater Chem C* (2018) 6(5):989–99. doi:10.1039/c7tc04486k
- Fan P, Zhong M, Bai B, Jin G, Zhang H. Tuning the Optical Reflection Property of Metal Surfaces via Micro-nano Particle Structures Fabricated by Ultrafast Laser. *Appl Surf Sci* (2015) 359:7–13. doi:10.1016/j.apsusc.2015.10.069
- Fan P, Wu H, Zhong M, Zhang H, Bai B, Jin G. Large-Scale Cauliflower-Shaped Hierarchical Copper Nanostructures for Efficient Photothermal Conversion. *Nanoscale* (2016) 8(30):14617–24. doi:10.1039/c6nr03662g
- Xu N, Hu X, Xu W, Li X, Zhou L, Zhu S, et al. Mushrooms as Efficient Solar Steam-Generation Devices. *Adv Mater* (2017) 29(28):1606762. doi:10.1002/adma.201606762
- Zhang T, Wang S-J, Zhang X-Y, Fu M, Yang Y, Chen W, et al. Recent Progress on Nanostructure-Based Broadband Absorbers and Their Solar Energy Thermal Utilization. *Front Chem Sci Eng* (2020) 15(1):35–48. doi:10.1007/s11705-020-1937-6
- Yang Z, Han X, Lee HK, Phan-Quang GC, Koh CSL, Lay CL, et al. Shape-Dependent Thermo-Plasmonic Effect of Nanoporous Gold at the Nanoscale for Ultrasensitive Heat-Mediated Remote Actuation. *Nanoscale* (2018) 10(34):16005–12. doi:10.1039/c8nr04053b
- Søndergaard T, Novikov SM, Holmgaard T, Eriksen RL, Beermann J, Han Z, et al. Plasmonic Black Gold by Adiabatic Nanofocusing and Absorption of Light in Ultra-sharp Convex Grooves. *Nat Commun* (2012) 3:969. doi:10.1038/ncomms1976
- Aslam U, Rao VG, Chavez S, Lincic S. Catalytic Conversion of Solar to Chemical Energy on Plasmonic Metal Nanostructures. *Nat Catal* (2018) 1(9):656–65. doi:10.1038/s41929-018-0138-x
- Bai S, Sugioka K. Recent Advances in the Fabrication of Highly Sensitive Surface-Enhanced Raman Scattering Substrates: Nanomolar to Attomolar Level Sensing. *Light: Adv Manufacturing* (2021) 2(2):186. doi:10.37188/lam.2021.013
- Zhai Y, Chen G, Ji J, Ma X, Wu Z, Li Y, et al. Large-Scale, Broadband Absorber Based on Three-Dimensional Aluminum Nanospine Arrays Substrate for Surface Plasmon Induced Hot Electrons Photodetection. *Nanotechnology* (2019) 30(37):375201. doi:10.1088/1361-6528/ab2158
- Meudt M, Jakob T, Polywka A, Stegers L, Kropp S, Runke S, et al. Plasmonic Black Metasurface by Transfer Printing. *Adv Mater Technol* (2018) 3(11):1800124. doi:10.1002/admt.201800124
- Berean KJ, Sivan V, Khodasevych I, Boes A, Della Gaspera E, Field MR, et al. Laser-Induced Dewetting for Precise Local Generation Of au Nanostructures for Tunable Solar Absorption. *Adv Opt Mater* (2016) 4(8):1247–54. doi:10.1002/adom.201600166
- Wen Z, Shi H, Yue S, Li M, Zhang Z, Wang R, et al. Large-Scale Black Silicon Induced by Femtosecond Laser Assisted with Laser Cleaning. *Front Phys* (2022) 10:10. doi:10.3389/fphy.2022.862605
- Hu A. *Laser Micro-nano-manufacturing and 3d Microprinting*. Springer (2020).
- Sopeña P, Arrese J, González-Torres S, Fernández-Pradas JM, Cirera A, Serra P. Low-Cost Fabrication of Printed Electronics Devices through Continuous Wave Laser-Induced Forward Transfer. *ACS Appl Mater Inter* (2017) 9(35):29412–7. doi:10.1021/acsami.7b04409
- Zhou W, Bai S, Ma Y, Ma D, Hou T, Shi X, et al. Laser-Direct Writing of Silver Metal Electrodes on Transparent Flexible Substrates with High-Bonding Strength. *ACS Appl Mater Inter* (2016) 8(37):24887–92. doi:10.1021/acsami.6b07696
- Sopeña P, Garcia-Lechuga M, Wang A, Grojo D. Ultrafast Laser Stabilization by Nonlinear Absorption for Enhanced-Precision Material Processing. *Opt Lett* (2022) 47(4):993–6. doi:10.1364/OL.449720
- Wang A, Jiang L, Li X, Xu Z, Huang L, Zhang K, et al. Nanoscale Material Redistribution Induced by Spatially Modulated Femtosecond Laser Pulses for Flexible High-Efficiency Surface Patterning. *Opt Express* (2017) 25(25):31431–42. doi:10.1364/OE.25.031431
- Bai S, Serien D, Ma Y, Obata K, Sugioka K. Attomolar Sensing Based on Liquid Interface-Assisted Surface-Enhanced Raman Scattering in Microfluidic Chip by Femtosecond Laser Processing. *ACS Appl Mater Inter* (2020) 12(37):42328–38. doi:10.1021/acsami.0c11322
- Ding C-F, Li L, Young H-T. Laser-Induced Backward Transfer of Conducting Aluminum Doped Zinc Oxide to Glass for Single-step Rapid Patterning. *J Mater Process Tech* (2020) 275:116357. doi:10.1016/j.jmatprotec.2019.116357
- Papazoglou S, Tsouti V, Chatzandroulis S, Zergioti I. Direct Laser Printing of Graphene Oxide for Resistive Chemosensors. *Opt Laser Tech* (2016) 82:163–9. doi:10.1016/j.optlastec.2016.03.009
- Munoz-Martin D, Brasz CF, Chen Y, Morales M, Arnold CB, Molpeceres C. Laser-Induced Forward Transfer of High-Viscosity Silver Pastes. *Appl Surf Sci* (2016) 366:389–96. doi:10.1016/j.apsusc.2016.01.029
- Mikšys J, Arutinov G, Römer GRBE. Pico- to Nanosecond Pulsed Laser-Induced Forward Transfer (Lift) of Silver Nanoparticle Inks: A Comparative Study. *Appl Phys A* (2019) 125(12):814. doi:10.1007/s00339-019-3085-8
- Boutopoulos C, Kalpyris I, Serpetzoglou E, Zergioti I. Laser-Induced Forward Transfer of Silver Nanoparticle Ink: Time-Resolved Imaging of the Jetting Dynamics and Correlation with the Printing Quality. *Microfluid Nanofluid* (2013) 16(3):493–500. doi:10.1007/s10404-013-1248-z
- Pohl R. Imaging of the Ejection Process of Nanosecond Laser-Induced Forward Transfer of Gold. *J Laser Micro/Nanoengineering* (2015) 10(2):154–7. doi:10.2961/jlmn.2015.02.0008
- Fardel R, Nagel M, Nüesch F, Lippert T, Wokaun A. Laser-Induced Forward Transfer of Organic Led Building Blocks Studied by Time-Resolved Shadowgraphy. *J Phys Chem C* (2010) 114(12):5617–36. doi:10.1021/jp907387q
- Liu Y, Zhang J, Shanguan S, Qi D, Sun T, Zheng H. Temporal-Spatial Measurement of Surface Morphological Evolution Time in Nanosecond Laser Irradiation on the Copper Film. *Front Phys* (2022) 10:10. doi:10.3389/fphy.2022.845576
- Li R, Yan J, Fang Y, Fan X, Sheng L, Ding D, et al. Laser-Scribed Lossy Microstrip Lines for Radio Frequency Applications. *Appl Sci* (2019) 9(3):415. doi:10.3390/app9030415
- Chakraborty I, Shirodkar SN, Gohil S, Waghmare UV, Ayyub P. The Nature of the Structural Phase Transition from the Hexagonal (4h) Phase to the Cubic (3c) Phase of Silver. *J Phys Condens Matter* (2014) 26(11):115405. doi:10.1088/0953-8984/26/11/115405
- Li R-Z, Hu A, Zhang T, Oakes KD. Direct Writing on Paper of Foldable Capacitive Touch Pads with Silver Nanowire Inks. *ACS Appl Mater Inter* (2014) 6(23):21721–9. doi:10.1021/am506987w

Conflict of Interest: The authors declare that the research was conducted in the absence of any commercial or financial relationships that could be construed as a potential conflict of interest.

Publisher's Note: All claims expressed in this article are solely those of the authors and do not necessarily represent those of their affiliated organizations, or those of the publisher, the editors, and the reviewers. Any product that may be evaluated in this article, or claim that may be made by its manufacturer, is not guaranteed or endorsed by the publisher.

Copyright © 2022 Li, Guo, Liu, Yang, Fang, Yu and Yan. This is an open-access article distributed under the terms of the Creative Commons Attribution License (CC BY). The use, distribution or reproduction in other forums is permitted, provided the original author(s) and the copyright owner(s) are credited and that the original publication in this journal is cited, in accordance with accepted academic practice. No use, distribution or reproduction is permitted which does not comply with these terms.